Difference imaging reveals ordered regions of RNA in turnip yellow mosaic virus

B Böttcher* and RA Crowther

Background: Turnip yellow mosaic virus (TYMV) is a small icosahedral plant virus with a capsid containing 180 subunits arranged with hexamer–pentamer clustering. Cross-linking studies have indicated extensive contacts between RNA and coat protein, suggesting that substantial parts of the RNA might be icosahedrally ordered.

Results: Comparison of maps computed to a Fourier cut-off of 1.5 nm from electron micrographs of ice-embedded specimens of TYMV and of empty capsids produced by freeze-thawing reveals strong inner features around the threefold axes in the virus but not in the empty capsid. Internal features of subunit packing indicate that interhexamer contacts are closer than those between pentamers and hexamers and that pentamer density in the empty capsid is reduced relative to that in the virus.

Conclusions: The differences between virus and empty capsid indicate that substantial parts of the RNA are icosahedrally ordered and that the exit of RNA on freeze-thawing is accompanied by the loss of at least one pentamer unit.

Address: Medical Research Council Laboratory of Molecular Biology, Hills Road, Cambridge, CB2 2QH, UK.

*Corresponding author.

Key words: cryo-electron microscopy, difference imaging, image processing, turnip yellow mosaic virus, RNA organization

Received: **15 Dec 1995**
Revisions requested: **8 Jan 1996**
Revisions received: **7 Feb 1996**
Accepted: **15 Feb 1996**

Structure 15 April 1996, **4**:387–394

Introduction

Turnip yellow mosaic virus (TYMV) is a member of the tymovirus family. It has a positive-stranded RNA genome with 6318 bases of which 96.9% are coding. The capsid is built of 180 copies of a 20 kDa coat protein organized with icosahedral T=3 symmetry and clustered in hexamers and pentamers [1]. The mean outer radius of the capsid was measured to be between 14 nm (by X-ray small-angle scattering [2]) and 15 nm (by cryo-electron microscopy) [3]. Neutron small-angle scattering showed that most of the RNA is buried inside a radius of 10–11 nm [4,5]. From X-ray diffraction it was predicted that significant parts of the RNA penetrate deeply into the protein shell at the positions of the 32 hexamer and pentamer morphological units, extending out to a radius of 12.5 nm [6]. The viral RNA contains about 38% cytosine and can be cross-linked at pH 7.3 after bisulphite treatment and ultraviolet irradiation mainly to two sites on the coat protein [7]. In the cross-linking experiments almost all of the protein subunits reacted with viral RNA.

Upon alkaline treatment or bulk freezing, the intact virus swells by 3–4% before complete release of RNA [4,8]: between five and nine coat protein subunits are lost [9,10]. The remaining protein maintains a spherical shell, which at neutral pH has the same outer dimensions as the virus [8]. It is likely that a similar loss of subunits occurs *in vivo* during infection of plants [11].

In this paper we present three-dimensional maps of TYMV and of the empty capsid computed to a Fourier cut-off of about 1.5 nm from electron micrographs of unstained frozen specimens. The maps confirm previous models of the overall organization of subunits in the outer part of the capsid but show that the subunits are dimer-clustered at inner radii. The difference map reveals the presence of ordered regions of RNA around the threefold axes and shows the sites of contact between the RNA and the inner surface of the capsid protein. Internal features of subunit packing suggest closer interactions between neighbouring hexamer units than between a pentamer and the surrounding hexamers. The density associated with a pentamer unit is lower in empty capsids than in the virus, indicating that exit of the RNA on freeze-thawing is accompanied by the loss of at least one pentamer unit.

Results

Micrographs

Figure 1 shows micrographs of TYMV and of empty protein capsids. The virus particles have a circular shape and appear to be filled (Fig. 1a). Empty capsids, which have released their RNA after freezing and thawing, have a more ring-shaped appearance (Fig. 1b). Some of these rings appear to be broken or incomplete but many of them seem to be intact.

In all micrographs used for reconstruction of TYMV, the rod-shaped tobacco mosaic virus (TMV) was also present (Fig. 1). The TMV particles were used to assess the quality of each micrograph (see Table 1). The TMV also allowed the determination of the size of TYMV and the empty capsids absolutely and independently. It was thus

Figure 1

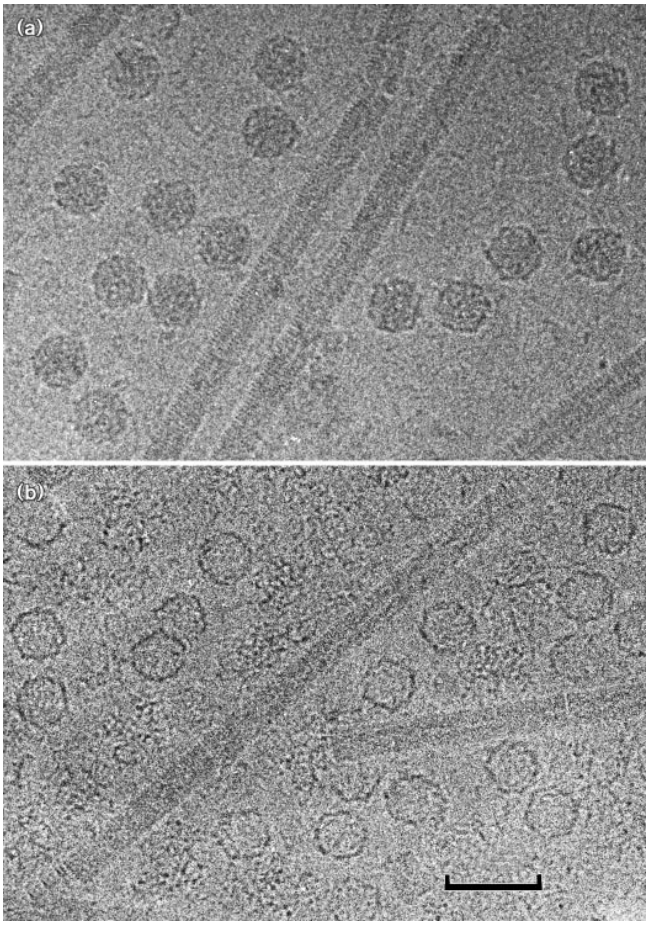

Micrographs of unstained specimens of **(a)** TYMV and **(b)** empty capsids produced by freeze-thawing. Rod-shaped TMV particles are present in both images for reference. Micrographs were taken at the Hitachi HF2000 at 200 kV and 60 000× magnification with the defocus in (a) Δ=2810 nm and in (b) Δ=1780 nm. Scale bar: 50 nm.

Table 1

Summary of imaging conditions and quality of micrographs used for TYMV reconstruction.

Micrograph number	1682	1671	1638	1670
Sum of TYMV transforms	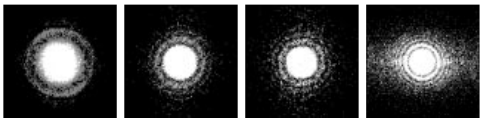			
Defocus (nm)	825	1485	1770	2810
Ctf zeros (nm):*				
observed	1.43,1.03	1.93,1.37	2.11,1.49	2.73,1.87
calculated	1.44,1.02	1.93,1.37	2.11,1.49	2.66,1.88
No. of TYMV particles included	85	30	20	45
Electron dose (e nm^{-2})	1200	950	1200	1000
TMV amplitude ratio 3/6 after ctf correction	1.7	2.6	1.9	2.0

Image quality was monitored by the ratio of the amplitudes of the 3rd to the 6th layerline of the best TMV on each micrograph after correction for the ctf. Electron diffraction indicates a true value for the ratio of amplitudes of 0.75 [21]. *For simplicity, only the positions of the first two zeros of the ctf are listed.

possible to check whether the empty shells had a different radius from that of the virus particles. In general micrographs taken at the Hitachi microscope show little contrast. However, it was possible to determine the orientation of these (sometimes barely visible) particles by using a set of reliable reference projections (see the Materials and methods section).

Three-dimensional maps

Three-dimensional maps of the virus and of the empty capsid are shown as surface representations in Figure 2. The maps, including data from 180 particles for the virus (Fig. 2a) and 56 particles for the empty capsid (Fig. 2b), were calculated to a Fourier cut-off of 1/1.5 nm^{-1}. The reconstructions show an icosahedral shell with T=3 symmetry. The 180 subunits are arranged in 32 knobs, 12 at the fivefold symmetry axes and 20 at the threefold symmetry axes. Indentations in the centres of the knobs at the threefold and fivefold symmetry axes can be observed. The maximum diameter of the particles is 30.1 nm for the knobs at the threefold axes and 31.2 nm at the fivefold axes. Small differences are apparent in the surface representations of the virus and the empty capsid, which we attribute to the much smaller number of particles used in the reconstruction of the latter. The difference map shows strong features at inner radii (Fig. 2c), which we attribute to ordered RNA (see below). When contoured at the same level, the difference map at outer radii (Fig. 2d) shows only tiny features around the pentamers.

Spherical sections of the reconstructions were calculated and projected. The 0.5 nm thick spherical slices were spaced radially by 0.5 nm starting at an outer radius of 16 nm and ending at an inner radius of 8.5 nm. Selected sections are shown in Figure 3. In the empty capsid, the density is confined to radii between 11 nm and 15.5 nm (Fig. 3, bottom row), whereas in the virus, density can also be observed at smaller radii (Fig. 3, top row).

The spherical sections of the empty capsid and the virus show that densities corresponding to the knobs at the fivefold symmetry axes protrude about 0.5 nm further out than densities corresponding to the knobs at the threefold symmetry axes. The knobs join together to form a continuous shell at an outer radius of about 13 nm. On the inner surface of the capsid (radius about 11.5 nm), the subunits become dimer-clustered. The two subunits forming the strict dimer are disposed

Figure 2

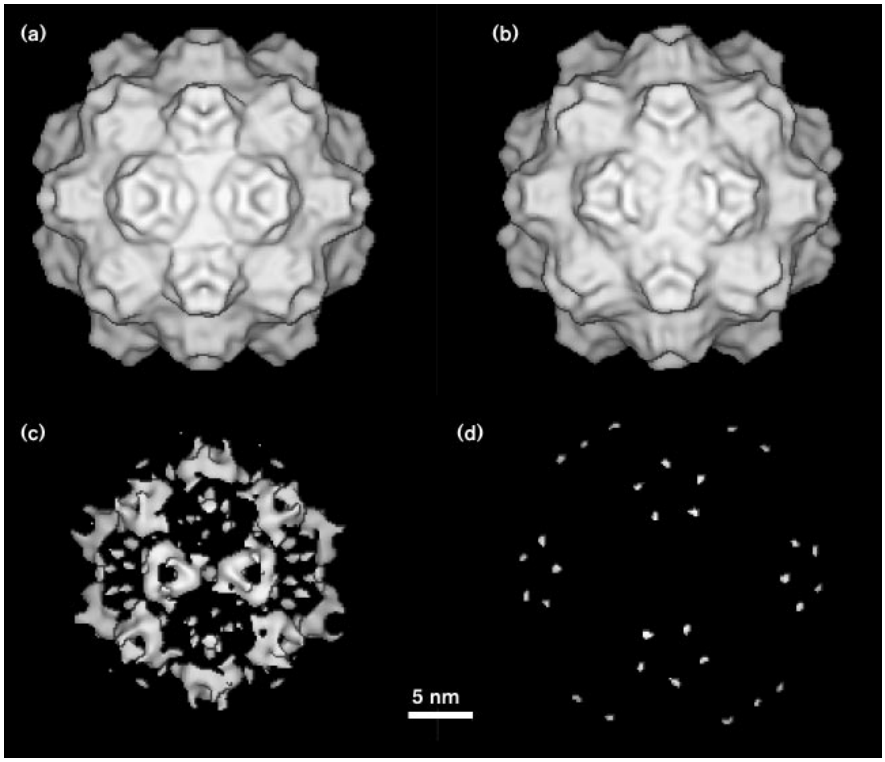

Surface representation of three-dimensional maps of TYMV. **(a)** Intact virus. **(b)** Empty capsid. Difference maps of virus minus empty capsid showing **(c)** radii 0–12.5 nm and **(d)** radii 12.5–16 nm. The maps, which are viewed down a strict twofold axis, were calculated to a Fourier cut-off of 1/1.5 nm^{-1}. All four plots were made at the same density threshold for the surface.

approximately towards the fivefold axes (see Fig. 4a). At radii between 12 nm and 12.5 nm (see Fig. 4b) four subunits from neighbouring hexamers (two from each) interlock closely across the strict twofold axes, whereas the neighbouring subunits from the pentamers are excluded from this interaction.

The knobs at the fivefold symmetry axes of the virus and of the empty capsid appear to be hollow with a small opening towards the outside of the virus. The opening widens towards the inside. The subunits at the tips of the knobs point towards each other at a radius of 15 nm. Measured relative to the density in hexamers, the density

Figure 3

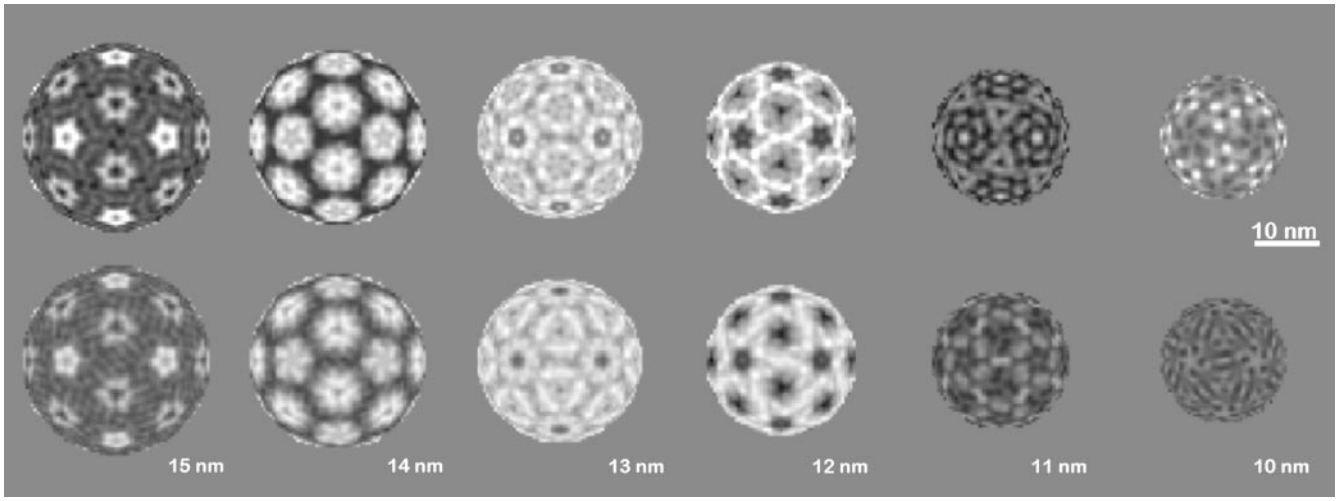

Spherical slices of the three-dimensional maps of TYMV. The intact virus is shown in the top row and the equivalent sections of the empty capsid in the bottom row. The slices are 0.5 nm thick and 1 nm apart starting at an outer radius of 15 nm, as indicated in the lower row. Density corresponding to protein and RNA is shown in white.

Figure 4

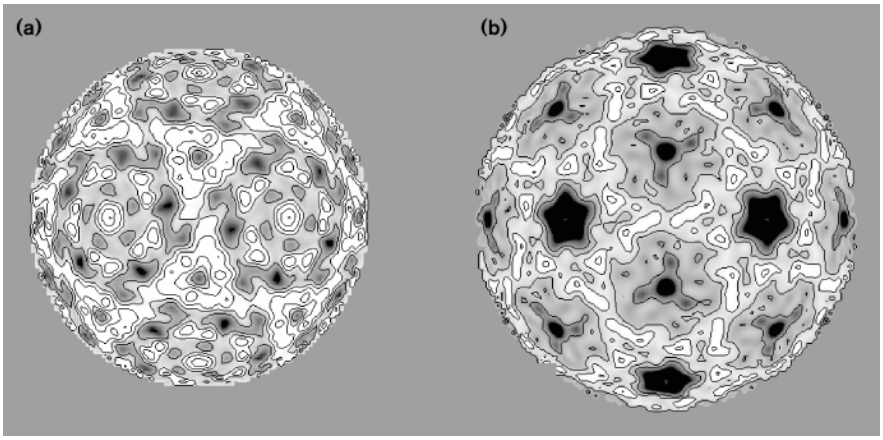

Two particular spherical slices of a three-dimensional map of TYMV. The map was calculated to a Fourier cut-off of 1/1.15 nm^{-1} and the sections correspond to radii of **(a)** 10.9 nm and **(b)** 12.2 nm. The sections were selected because the subunit packing and contacts between RNA and protein are displayed clearly.

of pentamers in empty capsids is 86% of that of pentamers in the virus, indicating that at least one pentamer has been lost in the empty capsids. At the threefold symmetry axes, the knobs have a hole or area of very low protein density in the centre running from the outside of the virus or empty capsid towards the inside, with its narrowest part at a radius of about 13.5 nm.

The most prominent features in the virus map at smaller radii are hollow triangles of density centred at the threefold symmetry axes (Fig. 4a). These triangles start at an inner radius of about 9.5 nm and are still faintly visible at an outer radius of 12 nm. No such features are present in the empty capsid and the background density in the empty capsid is on average much lower than in the virus. These hollow triangles centred on the threefold axes, which we believe correspond to ordered RNA, are the dominant features in the difference map computed by subtracting the capsid density from the virus density (Fig. 2c). Radial bridges of density extend from these triangles to the inner surface of the capsid at a radius of about 12–12.5 nm, as can be seen clearly when the difference map is superimposed on the map of the virus (Fig. 5).

Figure 5

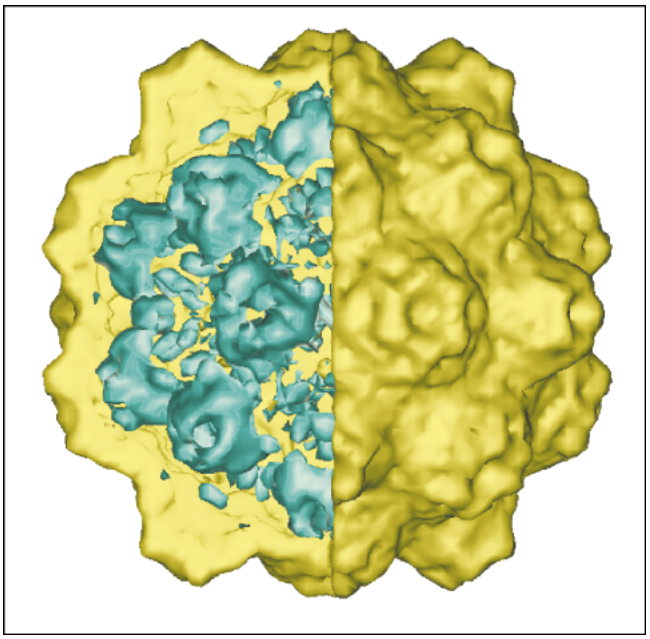

Superposition of the difference map (virus minus empty capsid) and the virus map. The surface representation of the difference map (see Fig. 2c) is placed inside the TYMV map (see Fig. 2a) but with one quarter of the TYMV map cut away. The density ascribed to RNA is represented in blue, the protein density in yellow.

Radial density

Radial density plots computed from the three-dimensional maps are shown in Figure 6. Protein density peaks occur at a radius of 12.5 nm in the virus reconstruction (Fig. 6a), as well as in the empty capsid reconstruction (Fig. 6b). The width of the protein peak is about 3 nm. For the virus reconstruction there is an inner peak at a radius of 9.5 nm, which is missing in the radial density of the empty capsid. This peak can be seen clearly in a plot of the difference between the radial densities of the virus and empty capsid reconstructions (Fig. 6c).

Contrast transfer function correction

In all reconstructions, images from micrographs with different defocuses were combined. Thus, information missing at the zeros of the contrast transfer function (ctf) in one micrograph was recovered from other micrographs included in the reconstruction. Nevertheless, a relatively strong Fresnel fringe remained which cannot be explained by the Fourier cut-off alone. Correction for 5–6% amplitude contrast according to [12] reduces, but does not eliminate, the Fresnel fringe. The remaining fringes are likely to be due to wrong correction at very low spatial frequencies, at which frequencies the expected contrast at all defocus values is small.

Figure 6

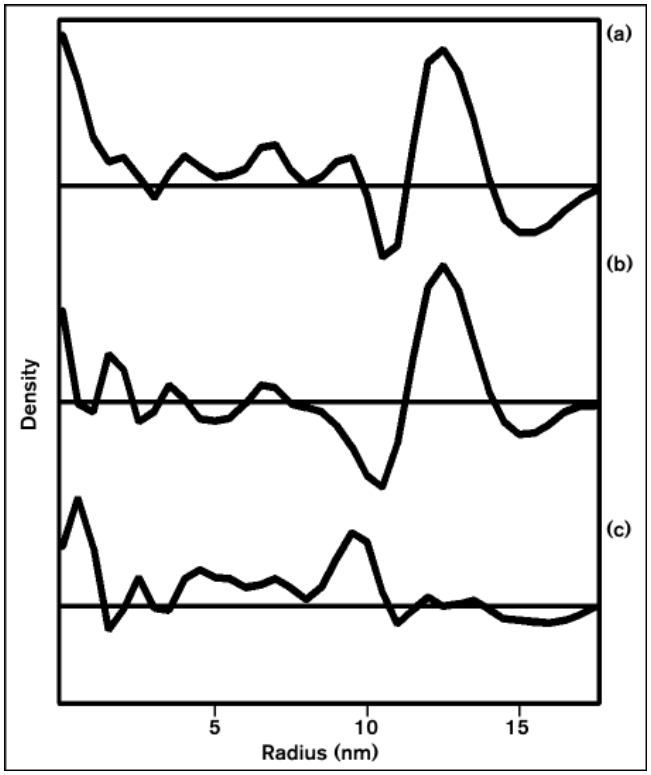

Radial density distributions in the three-dimensional maps. **(a)** TYMV. **(b)** Empty capsid. **(c)** The difference plot between virus and empty capsid density.

Figure 7

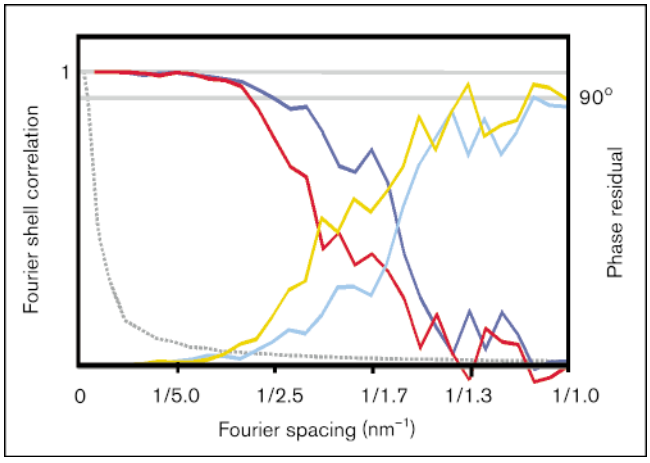

Assessment of the effective resolution of the maps. Weighted phase residual (right-hand scale, light blue and yellow traces), and Fourier shell correlation coefficient (left-hand scale, red and dark blue traces) plotted against Fourier spacing for TYMV (light and dark blue) and empty capsid (yellow and red). The significance level for the Fourier shell correlation coefficient is indicated by a dotted grey line.

Resolution

The effective resolution was determined by dividing the particles into two sets (for both the virus and the empty capsid), computing two independent three-dimensional maps of each, and determining the Fourier shell cross correlation and phase residuals [13]. The phase-residual plots and the Fourier shell cross-correlation plots are approximately mirror related and reach the 85° phase residual and significance level respectively at about the same Fourier spacing (Fig. 7), as found in a recent comparison of the two measures [14]. Both methods to determine resolution basically yield the same result.

In the maps used for difference imaging, a Fourier cut-off of 1/1.5 nm^{-1} was applied. At this Fourier spacing, both maps had a weighted phase residual of less than 70° giving quite reliable information. The resolution of the map of empty capsids is worse than that of the complete virus particle (Fig. 7). This difference probably reflects the smaller number of particles included in the empty capsid map rather than disruption of the capsid organization. Indeed, if the number of particles in the virus reconstruction is reduced to that in the empty capsid reconstruction, almost the same plots are obtained for the virus as for empty capsid (data not shown). Thus, the resolution is strongly dependent on the number of particles included in the reconstruction. The TMV particles in the same micrograph show a clear sixth layerline (spacing 1/1.15 nm^{-1}) in optical diffraction, which indicates that the micrographs should be suitable for determining the structure of TYMV to at least 1/1.15 nm^{-1}, if a sufficient number of particles is included.

Discussion

Protein organization in the capsid

The maps computed from the unstained TYMV particles show the same external hexamer–pentamer clustering as was found in negatively stained specimens by model building [1] or by computation [15]. However the use of unstained specimens permits the visualization of internal structures, in this case the inner dimer clustering of the protein subunits and a set of features that we believe, on the basis of differences between virus particles and empty capsids, correspond to RNA.

Intact virus and empty capsids have the same maximal outer dimensions of 30–31 nm, in good agreement with a previous cryo-electron microscopy study [3]. The knobs at the fivefold axes extend slightly further than those at the threefold axes, as was found in a map computed from negatively stained specimens [15].

The apparent radii of TYMV and its empty capsid were determined by photon correlation spectroscopy [8]: the complete virus yielded an average radius of 14.6 nm, somewhat smaller than the maximal dimensions reported here. Upon alkaline treatment, TYMV loses about six

subunits [10] and swells by about 4% [8] before complete release of its RNA. Upon return to pH 7.0, the average radius decreases again to 14.6 nm [8]. TYMV also loses between five and nine subunits and releases its RNA upon freeze-thawing [9]. It is likely that the mechanisms in both cases (alkaline treatment and freeze-thawing) are similar. It is therefore expected that viruses and empty capsids have the same outer dimensions under the imaging conditions chosen, in agreement with our observations here. No swelling of the virus is apparent at 100 K, in contrast to that observed by neutron small-angle scattering of bulk-frozen TYMV at 80 K [4].

At outer radii (13–15 nm), the subunits interact strongly to form hexamer and pentamer units. At smaller radii (12.5–13 nm), the subunits join to form a more continuous shell of density protecting the RNA. On the inner surface of the capsid the subunits are disposed in a dimer-clustered manner, leaving large holes around the fivefold and threefold axes (Fig. 3, bottom row, 11 nm radius). The details of subunit packing support the idea that it is pentamer units that are lost on freeze-thawing.

Four subunits from neighbouring hexamer units (two from each) seem to interlock across the strict twofold axis at a radius of 12–12.5 nm to form a closely packed feature, whereas the subunits from the pentamers stay separate (Fig. 4b). Thus, except for interaction at internal radii, the pentamer units are clearly separated from the frame composed of hexamerically arranged subunits. It is therefore likely that upon freeze-thawing a knob at one of the fivefold symmetry axes is lost rather than one from one of the threefold axes. This is supported by the finding, that relative to the hexamers, the protein density of the pentamers in the empty capsids at radii between 13.5 nm and 15 nm is 86% of that observed in the virus. This corresponds to an average loss of about eight subunits, which is in agreement with [9]. This indicates that, on average, the virus loses at least one pentamer morphological unit and that it is unlikely that any loss of knobs occurs at the threefold axes. A similar loss of subunits occurs during uncoating *in vivo* [11].

Difference imaging shows ordered RNA

The difference plot of the radial density distributions between viruses and empty capsids shows no substantial amount of density at radii greater than 11 nm, which is in agreement with earlier small-angle neutron scattering data collected from viruses at room temperature, for which no RNA could be found at radii greater than 10–11 nm [4,5].

The strongest features in the difference map between the virus and the empty capsid are hollow triangles of density centred on each of the threefold axes. These triangles of density, which we ascribe to segments of ordered RNA, extend outwards to partly fill the threefold holes on the inside of the capsid. The overall length of the edge of the triangle is about 5.5 nm and the thickness about 2 nm. At a radius of 11 nm each triangle of density appears to make close contact with one subunit in each of the three neighbouring strict dimers and a glancing contact with one subunit in each of the three neighbouring local dimers (Fig. 4a). At a larger radius (12–12.5 nm) there are radial bridges of density to the inner surface of the capsid (Fig. 5). These may be RNA or perhaps loops of protein interacting with the RNA, which are ordered in the virus but disordered in the empty shell.

The difference map also shows a weaker feature on the fivefold axes. While this might represent residual noise in the map, there is good reason to think that it arises from partly ordered RNA. The hole on the fivefold axes is only 3.5 nm in diameter, which could accommodate only one double-helical RNA stem. The contacts made by the triangles of RNA at the threefold axes leave one protein subunit in each local dimer unsatisfied, with the equivalent contact surface pointing towards the fivefold axis. If one out of five of these sites around the fivefold axes were occupied on a random basis, averaging would give rise to a weak feature on the fivefold axes.

Our observations agree with the general model of Klug *et al.* [6], who proposed that RNA 'bunches' penetrate the capsid at the fivefold and threefold axes to an effective outer radius of 12.5 nm. This coincides with the radius of the radial bridges of density at the threefold axes in our map. However, the ordered RNA only touches the protein and is clearly not embedded in the protein capsid (Fig. 5), as proposed earlier [6]. The contact occurs at two distinct sites on the protein subunit, one at a smaller radius of about 11 nm where the hollow RNA triangles make a sliding contact to the surrounding protein subunits at the strict and local twofold axes, and the other at a radius of about 12–12.5 nm in the form of radial bridges. These two sites might correspond to the two regions in the protein subunit that were identified by cross-linking experiments [7].

Biological implications

The capsid of turnip yellow mosaic virus (TYMV) consists of 180 copies of a single coat protein that forms a spherical shell around the 6.3 kb genomic RNA. The coat protein extends from an inner radius of about 11 nm to an outer radius of about 15.5 nm. At outer radii, the subunits are clustered into 12 pentamer and 20 hexamer morphological units, which lie at the icosahedral fivefold and threefold axes respectively.

TYMV is a good model for studying protein–RNA interactions in viruses, because cross-linking experiments have demonstrated that specific contacts occur between RNA and protein. By comparing empty capsids (produced by freeze-thawing) with intact

virus particles, we have shown that at the threefold axes a hollow triangle of RNA makes two contacts to each of the surrounding subunits but does not otherwise penetrate the capsid protein. The dimensions of the RNA triangle are sufficient to accommodate a double-helical RNA rod at each side, oriented tangentially to the inner surface of the capsid. A weaker feature seen at the fivefold axes could be a partially ordered double-helical RNA rod arranged perpendicular to the surface of the capsid.

The capsid is formed of only one type of subunit. These subunits must be arranged in such a way that a stable spherical shell can be maintained whilst permitting release of RNA during infection. The release appears to occur by loss of some protein subunits. (*In vitro,* freeze-thawing or alkali treatment initiates a similar protein loss.) Different kinds of interactions between subunits are probably responsible for allowing these apparently conflicting requirements to be met. At outer radii, hexamer–pentamer clustering occurs but at inner radii the subunits are dimer-clustered across the strict and local twofold axes. In between these radial extremes the subunits from the pentamers are clearly separated from the subunits of the hexamers, with the latter forming an interlocked arrangement of four subunits across the strict twofold axes, involving two subunits from each hexamer. This shows that a single type of subunit is able to make geometrically very different contacts with neighbouring subunits. From the observed arrangement of the subunits and the relative density distribution in the empty capsid and the virus, it appears that after freeze-thawing one or two pentamers are lost. In contrast, the subunits forming the hexamers at outer radii build a very stable framework at inner radii which maintains the integrity of the spherical shell. Presumably this provides a mechanism whereby a stable capsid can, under relatively mild conditions, release the RNA during infection.

Materials and methods

Sample preparation

Before freezing, TYMV was mixed with TMV to act as an internal calibration. Virus concentrations in the mixed sample were about 10–20 mg ml^{-1} for each virus. Samples were frozen according to [16] with a freezing device as described in [17]. The device was placed in a cold room and the chamber was humidified by two water-soaked sponges to prevent evaporation from the sample. The grids were glow discharged in air and used within 1 h. The sample (2 μl) was applied onto a 400 mesh copper-rhodium grid (Agar Scientific, Stansted, UK) coated with a perforated carbon film. Some of the grids were covered with an additional very thin carbon film to reduce charging and allow thinner films of ice. Most of the sample was removed by blotting with two layers of filter paper (Whatman, Maidstone, UK) for 12–17 s. Immediately after blotting, the grid was plunged into liquid ethane by a spring-driven device. The ethane was prevented from freezing by a heater. Samples were also prepared without the heater. No difference with respect to the vitrification of the water was observed.

Empty capsids were prepared according to [3]. The virus suspension (2 μl) was applied to a grid, which was dipped into liquid nitrogen until the solution was completely frozen. The sample was then allowed to thaw on the grid at 4°C, after which the grid was prepared as described above.

Electron microscopy

Micrographs were taken under low-dose conditions at nominal magnifications of 36 000 and 60 000 at a Philips EM420 (Philips Electron Optics, Eindhoven, The Netherlands) operating at 120 kV or at 60 000× at a Hitachi HF2000 (Hitachi Ltd., Tokyo, Japan) microscope operating at 200 kV which was equipped with a field emission filament. At both microscopes Gatan cryo stages (Gatan Inc., Pleasanton, CA) were used. A temperature between 95 K and 100 K was maintained. Images were recorded on Kodak SO163 film (Eastman Kodak Company, Rochester, NY), which was developed for 12 min in full strength Kodak D19 developer.

Image processing

TMV particles were scanned with a modified Joyce Loebl densitometer (Joyce Loebl, Gateshead, UK) to judge the quality of the micrographs. A step size of 10 μm was used corresponding to approximately 0.17 nm per pixel at specimen level. Parts of the TMV were boxed with a narrow box with a length between 100 nm and 150 nm. After background subtraction, a Fourier transformation was computed. From the transform the intensities of the third and sixth layer lines were determined. The intensities were corrected for the contrast transfer function (ctf) and the envelope function due to spatial coherence [18] and used to judge the quality of the micrographs used.

TYMV particles were scanned using either a Nikon or a Joyce Loebl densitometer. A step size of 20 μm/pixel was used. For calibration of the magnification, TMV on the same image was scanned using the same settings of the densitometer. A Fourier transform was computed of the TMV. From the positions of the third and sixth layerlines (1/2.3 nm^{-1} and 1/1.15 nm^{-1}) the magnification was calculated and particles from different images scaled respectively.

The centres of the TYMV particles were first determined by cross correlation to a Gaussian ring with the same diameter as the virus and the width of the ring roughly corresponding to the width of the capsid. Subsequently, the origins of new particles were determined by cross correlation to a sum of eight different projections of an existing map.

The particles were boxed with a circular box with a radius of 20.8 nm and the pre-determined centre. The background was subtracted and the grey value distribution was normalized. For the first reconstruction, focus pairs taken at 36 000× magnification and a defocus of about 1000 nm and 2000 nm at the Philips EM420 were chosen. The orientations of the higher defocused particles were determined using self-common lines [19]. The orientations found were then used for images of smaller defocus. The reliability of the orientations was judged by computation of a low-resolution two-particle three-dimensional reconstruction between a reference particle and each other particle in the data set [20]. The preservation of the threefold symmetry in the projections along the threefold symmetry axis was used as the main criterion for accepting an orientation. Then a map was calculated from these particles. Further refinement of the origin and angles of view was performed using cross-common lines to three projections of the calculated map [20].

With the current set of programs for making three-dimensional maps of icosahedral viruses, it is difficult to incorporate proper ctf corrections for combining data from micrographs taken at different defocuses. We have partly overcome this difficulty by computing separate three-dimensional maps from images at each particular defocus and by then combining these three-dimensional maps with appropriate corrections for the defocus, although this approach does not deal with astigmatism. The correction is done by computing the three-dimensional Fourier transform of each map and then estimating the true value of each frequency component by a weighted combination of the observed

values of that component. The contrast transfer function, *c*, incorporating amplitude and phase contrast is of the form:

$$c = a\cos\chi + \sqrt{(1-a^2)}\sin\chi,$$

where *a* is the fractional amplitude contrast and χ is the phase shift. If F_i is the observed value of a particular frequency component in the transform of the i^{th} map, then the true value of this component *F* is estimated by:

$$F = \frac{\sum_i c_i w_i F_i}{\sum_i c_i^2 w_i F_i + f}$$

Here c_i is the value of the ctf at this frequency in the i^{th} transform and w_i is an overall fractional weight (Σw_i=1) for the i^{th} map which reflects its reliability (e.g. the number of particles included). The term *f*, akin to the signal-to-noise ratio in a Wiener filter, prevents over amplification of terms when the rest of the denominator is small. In our case where we combine images with several different defocuses, *f* has its principal effect at very low spatial frequencies, where it sets the average density level in the final three-dimensional map computed by back transformation. *f* was adjusted to give an average radial density value of zero inside and outside the empty capsids. The same filter was used for the corresponding virus reconstructions. For the amplitude contrast, a value of 5% was used for images from the Hitachi.

When using projections of the computed map as a basis for determining or refining the orientation parameters of particles, it is important for the computed projections to have a defocus applied that matches that of the image. This can be done, as above, by using the three-dimensional transform but in this case simply multiplying by the appropriate ctf and back-transforming, before computing the projections.

Existing maps were used as references to find the orientations of particles in micrographs taken under different conditions. For example, the map of the images taken at the Philips EM420 at 36 000× was scaled and then used as a reference to find the first orientations of the particles from micrographs taken at the Hitachi HF2000 at 200 kV and a magnification of 60 000×. The resulting orientations were used to calculate a preliminary map from these particles. For further refinement of the orientations, only maps resulting from micrographs taken at the Hitachi microscope were used as reference.

Difference maps

Reconstructions were calculated for empty capsids and the complete virus to the same resolution. In order to determine the density scaling of the virus relative to the empty capsid, it was necessary to determine whether subunits had been lost from the empty capsid. This was done by integrating the density over radii greater than 13 nm in a pentamer unit and a hexamer unit in the maps of both the virus and the empty capsid. The ratio of pentamer density to hexamer density was lower in the empty capsid than the virus indicating that pentamer units had been lost in the empty capsid. The density of the empty capsid reconstruction was first scaled to give the same integral peak for the radial density distribution for radii between 11.5 nm and 15.5 nm. Before subtraction from the virus map the density of the empty capsid map was weighted by a factor of 1.05 to adjust for the subunit loss. The features in the difference map were not strongly dependent on the precise way in which the scaling was done.

Resolution

For an estimate of resolution, data sets were divided randomly into two equal subsets. From each subset a map was calculated. Fourier shell correlation coefficients and weighted phase residuals were calculated between maps according to [13] (equations 3 and 6, respectively).

Acknowledgements

We thank Dr PJG Butler for providing TMV and TYMV and Dr JT Finch for comments on the manuscript. BB was supported by an EMBO long term fellowship (ALTF 673–1993) and an EEC human capital and mobility grant (ERB4001GT931348).

References

1. Finch, J.T. & Klug, A. (1966). Arrangement of protein subunits and the distribution of nucleic acid in turnip yellow mosaic virus: II. Electron microscopic studies. *J. Mol. Biol.* **15**, 344–364.
2. Schmidt, P., Kaesberg, P. & Beeman, W.W. (1954). Small-angle X-ray scattering from turnip yellow mosaic virus. *Biochim. Biophys. Acta* **14**, 1–11.
3. Adrian, M., Timmins, P.A. & Witz, J. (1992). *In vivo* decapsidation of turnip yellow mosaic virus investigated by cryo-electron microscopy: a model for the decapsidation of a small isometric virus. *J. Gen. Virol.* **73**, 2079–2083.
4. Witz, J., Timmins, P.A. & Adrian, M. (1993). Organization of turnip yellow mosaic virus investigated by neutron small-angle scattering at 80 K: an intermediate state preceding decapsidation of the virion? *Proteins* **17**, 223–231.
5. Jacrot, B., Chauvin, C. & Witz, J. (1977). Comparative neutron small-angle scattering study of small spherical RNA viruses. *Nature* **266**, 417–421.
6. Klug, A., Longley, W. & Leberman, R. (1966). Arrangement of protein subunits and the distribution of nucleic acid in turnip yellow mosaic virus: I. X-ray diffraction studies. *J. Mol. Biol.* **15**, 315–343.
7. Ehresmann, B., Briand, J.-P., Reinbolt, J. & Witz, J. (1980). Identification of binding sites of turnip yellow mosaic virus protein and RNA by crosslinks induced *in situ*. *Eur. J. Biochem.* **108**, 123–129.
8. Keeling, J., Collins, E.R. & Matthews, R.E.F. (1979). Behaviour of turnip yellow mosaic virus nucleoproteins under alkaline conditions. *Virology* **97**, 100–111.
9. Katouzian-Safadi, M., Berthet-Colominas, C., Witz, J. & Kruse, J. (1983). Evidence for the presence of a hole in the capsid of turnip yellow mosaic virus after RNA release by freezing and thawing: decapsidation of turnip yellow mosaic virus *in vitro*. *Eur. J. Biochem.* **137**, 47–55.
10. Keeling, J. & Matthews, R.E.F. (1982). Mechanism for release of RNA from turnip yellow mosaic virus at high pH. *Virology* **119**, 214–218.
11. Matthews, R.E.F. & Witz, J. (1985). Uncoating of turnip yellow mosaic virus RNA *in vivo*. *Virology* **144**, 318–327.
12. Toyoshima, C., Yonekura, K. & Sasabe, H. (1993). Contrast transfer for frozen-hydrated specimens II. Amplitude contrast at very low frequencies. *Ultramicroscopy* **48**, 165–176.
13. van Heel, M. (1987). Similarity measures between images. *Ultramicroscopy* **21**, 95–100.
14. de la Fraga, L.G., Dopazo, J. & Carazo, J.M. (1995). Confidence limits for resolution estimation in image averaging by random subsampling. *Ultramicroscopy* **60**, 385–391.
15. Mellema, J.E. & Amos, L.A. (1972). Three-dimensional image reconstruction of turnip yellow mosaic virus. *J. Mol. Biol.* **72**, 819–822.
16. Dubochet, J., *et al*., & Schultz, P. (1988). Cryo-electron microscopy of vitrified specimens. *Quart. Rev. Biophys.* **21**,129–228.
17. Bellare, J.R., Davis, H.T., Scriven, L.E. & Talmon, Y. (1988). Controlled environment vitrification system: an improved sample preparation technique. *J. Electron Microsc. Tech.* **10**, 87–111.
18. Reimer L. (1993). *Transmission Electron Microscopy*. pp. 224–229, Springer Verlag, Berlin and Heidelberg.
19. Crowther, R.A. (1971). Procedures for three-dimensional reconstruction of spherical viruses by Fourier synthesis from electron micrographs. *Philos. Trans. R. Soc. (Lond) B* **261**, 221–230.
20. Crowther, R.A., *et al*., & Pumpens, P. (1994). Three-dimensional structure of hepatitis B virus core particles determined by electron cryomicroscopy. *Cell* **77**, 943–950.
21. Cyrklaff, M. & Kühlbrandt, W. (1994). High-resolution electron microscopy of biological specimens in cubic ice. *Ultramicroscopy* **55**, 141–153.